3D PRINTING AND ADDITIVE MANUFACTURING
Volume 5, Number 2, 2018

DOI: 10.1089/3dp.2017.0054

ORIGINAL ARTICLE

Polyelectrolyte Soft Actuators: 3D Printed Chitosan and Cast Gelatin

Ali Zolfagharian, Akif Kaynak, Sui Yang Khoo, and Abbas Z. Kouzani

Abstract

With increasing utilization of robots in daily tasks, especially in biomedical and environmental monitoring applications, there would be demands for soft, biodegradable, or even edible actuators that provide more versatility than conventional rigid materials (e.g., metals and plastics). Polyelectrolyte hydrogels produce mechanical motion in response to electrical stimulus, making them good candidates for implementation of soft actuators. However, their conventional fabrication process has so far hindered their applicability in a broad range of controlled folding behaviors. A novel application of 3D printing in biodegradable and biocompatible soft robots is presented in this study. It is observed that the contactless electroactive polyelectrolyte structures demonstrate reversible bending through polarity changes of electrodes. Edible gelatin and chitosan hydrogels are chosen as potential candidates of polyelectrolyte actuators. Actuation of 3D printed chitosan and its performance are compared with those of conventional cast film gelatin. The printing parameters are optimized for fabrication of the desired geometrical model and the printing effects on actuation performance are analyzed. It is demonstrated that the rectilinear hollows made by 3D printing improve the functionality of actuation in chitosan compared with a cast film gelatin actuator. 3D printed polyelectrolyte actuators will open a new chapter of soft biodegradable robots for preserving sustainability while offering custom geometrical, functional, and control properties.

Keywords: soft actuator, 3D printing, polyelectrolyte hydrogel

Introduction

The advent of 3D printing and soft robotics is a viable prospect for robotic and medical scientists to develop renewable custom-designed soft actuators for accomplishing designated tasks. A current challenge of soft robots is the recalling phase of such robots deployed in the bioenvironment. A possible interesting solution might be development of soft robots made of biologically compatible and biodegradable actuators. However, accessibility and cost of materials to be used for such actuators along with repeatability of using them are factors to consider. Recent achievements in harvesting electrical energy through microbial fuel cells are a good prospect for further development of low-voltage electrical stimulus biodegradable soft robots.[1,2] Biodegradable soft actuators known as edible actuators were recently introduced and have drawn attention due to their application as less invasive electronic capsules in monitoring the internal organs.[3] Also, an electrically sensitive hydrogel has been tested in a saline solution as a controllable cancer drug release application under a range of voltages from 0 to 20 V.[4] These innovations have tempted the development of electrically stimulated contactless polymer soft actuators capable of actuating in a similar voltage range.

The biocompatibility and biodegradability of the polymer for soft actuators are, respectively, the primary and secondary measures to be considered. Among available polymers, the ideal choice for soft actuators is one that possesses both biocompatibility and biodegradability while being a natural polymer rather than a synthetic polymer.[2] It has always been a challenge to find artificial polymers that possess both biocompatibility and biodegradability. The application of synthesized hydrogels in biological and pharmaceutical fields is quite limited due to their poor biocompatibility.[5–7] Therefore, degradable natural hydrogels (e.g., hydrogels made of soy protein or onion) are promising materials for creating renewable and sustainable soft actuators.[8,9]

Biodegradable soft robots powered by polyelectrolyte actuators are a primary choice for these applications. Gelatin

School of Engineering, Deakin University, Geelong, Australia.

and chitosan hydrogels are prevalent polyelectrolyte hydrogels with chemically bonded ionizable groups in their network.[10] They show mechanical responses due to electrical stimulus in an electrolyte solution and, therefore, can be used to produce soft actuators that can be controlled by the duration and strength of the applied electric stimulus.[11–14] In this sense, gelatin actuators respond well to natural dehydration and a ''hibernation state'' with no decomposition.[2] Gelatin is a biocompatible and biodegradable polyelectrolyte hydrogel, which is suitable for biomedical applications and was referred to as ''throw-away'' robot.[2] Chitosan is also a natural amphoteric hydrogel obtained from the deacetylation of chitin, the world's second most abundant natural polymer, with proven biomedical applications in wound healing, tissue engineering, and drug delivery.[10,15] Chitosan has already been investigated as a candidate for electroactive polymers for the actuation performance.[16]

The fabrication of soft actuators has always been challenging especially in small size while adhering to intricate geometrical design and preserving their structural integrity. This can be achieved by using 3D printing in the fabrication of soft actuators as this technology of digital fabrication enables precise construction of complex objects directly from a computer-aided design (CAD) model, thus enabling development of intricate actuators with less fabrication and postprocessing time, and least amount of waste material and lower cost.[17] That is, the 3D printed soft actuators can be fabricated by 3D printers with custom geometrical, functional, and control properties.[18–20] The ability to adjust the material properties during printing eliminates the need to design and print separate parts of the soft actuator and then attach them together.[20–25]

This study employs a 3D printer to develop polyelectrolyte actuators and reveals the early advantages of this fabrication method in a comparison study with two different polyelectrolyte hydrogels, gelatin from porcine skin and chitosan. The actuation performance of solid link gelatin and chitosan is compared with the 3D printed chitosan.

Mechanism of Actuation

Polyelectrolyte hydrogels show an electro-osmotic swelling response as a function of charge density and external salt concentration. The electro-osmotic effect is established when the electric field distributes the mobile ions asymmetrically between the gel and solution, inducing osmotic pressure differences that deform the gel. Immersing hydrogel structure in saline solution creates a chemical gradient between the mobile ions in the solution and the mobile counterions within the gel. Polyelectrolyte chains such as chitosan contain both carboxylic acid (-COOH) and amine ($-NH_2$) pendant groups. In alkaline condition, carboxylic moieties deprotonate to form negatively charged carboxylate groups. Once current is applied, the external field formed between cathode and anode electrodes creates a chemical potential that causes the electrolyte counter ions (Na^+ and OH^-) to migrate toward electrodes of opposite charges. In the middle of the way, however, the negatively charged chitosan film is placed that allows selective diffusion of Na^+ but blocks OH^- ions from crossing over. This condition eventuates in rapid increase of the OH^- concentration on one side of the film that faces the negative electrode. The polyelectrolyte film then acts as a semipermeable membrane for which the difference in concentration of hydroxyl ions on different sides of the membrane causes the increase in osmotic pressure across the membrane. Therefore, the film swells and bends toward the negative electrode. This phenomenon is known as Donnan effect. As per the Donnan equilibrium, the number of oppositely charged ions on each side of the gel–solution interface remains balanced to maintain electroneutrality within the system. At equilibrium, the chemical potential of the ions inside the gel equals the chemical potential of the ions in the external solution.[26,27]

Anionic gels will be bent toward cathode electrode in a buffer medium. This along with water electrolysis results in the pH reduction at the anode, which may protonate the carboxylic acid group in the gel and cause deswelling of the gel network. As for the anionic gel, the counterions migrate to the cathode causing a difference in ionic strength between inside and outside of the hydrogel, which, in turn, results in the osmotic pressure of the hydrogel close to the anode to be greater than the osmotic pressure of the hydrogel near the cathode. Thus, the gel near the anode swells, causing it to bend toward the cathode.

According to Flory's theory of polyelectrolytes in solutions,[28–30] the osmotic pressure (π) caused by ionic distribution is

$$\Pi_{ion} = RT\left(\sum_i C_i^{in} - \sum_i C_i^{out}\right), \tag{1}$$

where R is the gas constant, T is the absolute temperature, C_i^{in} is the concentration of mobile ion i in the gel, and C_i^{out} is the concentration of mobile ion i in the surrounding solution. This difference in ionic concentrations induces an osmotic pressure difference $\Delta\pi$ between the anode and cathode sides of the hydrogel, thus generating the driving force for the deformation of the hydrogel:

$$\Delta\Pi_{ion} = \pi_1 - \pi_2, \tag{2}$$

where π_1 represents the osmotic pressure between the hydrogel and the solution on the anode side and π_2 represents the osmotic pressure between the hydrogel and the solution on the cathode side (Fig. 1). For the polyanionic hydrogel, π_1 increases to give $\Delta\pi > 0$, such that the hydrogel swells on the anode side and shrinks on the cathode side, causing it to bend toward the cathode side. Conversely, for the polycationic hydrogel, as the osmotic pressure difference $\Delta\pi < 0$, the hydrogel bends toward the anode side.

In a system with i kinds of cations and j kinds of anions, $\Delta\pi$ is expressed as follows[30]:

$$\begin{aligned}\Delta\pi = {} & 2RT\sum_i\left[C_{i,c} + C_{i,B}\frac{V_B}{V_C}h_i t + C_{i,B}\frac{V_B}{V_C}h_i{}^2t^2 - C_{i,A}(1-h_i t)\right] \\ & - 2RT\sum_j\left[C_{j,c} + C_{j,B}\frac{V_B}{V_C}h_j t + C_{j,B}\frac{V_B}{V_C}h_j{}^2t^2 - C_{j,A}\left(1-h_j t\right)\right],\end{aligned} \tag{3}$$

where $C_{i,x}$ is the ion concentration of species i in the x part, $x = A,\ B,\ C$ as anode side electrolyte, gel, and cathode side electrolyte, respectively, at time $t = 0$, $\mathbf{h_i}$ is the transport rate of species i between parts. This osmotic pressure difference is

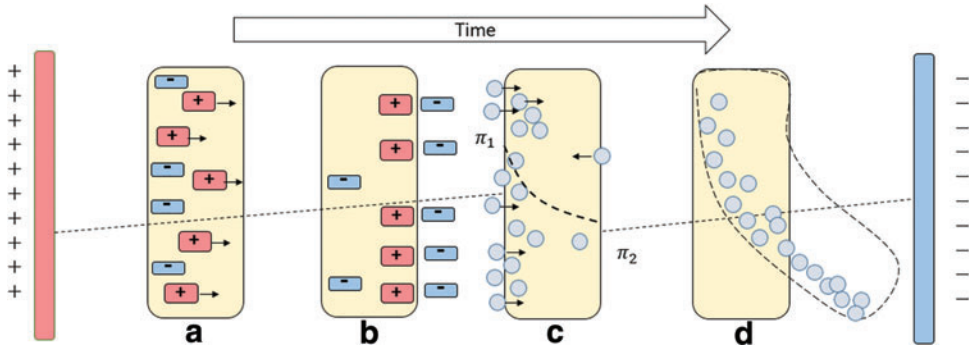

FIG. 1. Actuation mechanism illustration of polyelectrolyte actuators; **(a)** counterions migration **(b)** π_1 of anode side becomes larger than π_2 of cathode side, **(c)** more diffusion in anode side, **(d)** bending of the gel toward cathode. Color images available online at www.liebertpub.com/3dp

the main cause of bending. Assuming that actuator bending occurs as a three-point mechanical bending, the maximum tensile stress, σ, could be equated to $\Delta\pi$ and derived as

$$\Delta\pi = \frac{6DEY}{L^2}, \tag{4}$$

where E is Young's modulus, Y is the deflection, D is the thickness, and L is the initial length of the actuator. Using Equations (3) and (4), the deflection and the bending direction can be determined.

Materials and Methods

This study was conducted according to the following procedure. The materials were prepared and the cast actuators fabricated. 3D printing parameters were optimized based on shape fidelity of printed strand to fabricate the 3D printed chitosan hydrogel. Having fabricated both 3D printed and cast actuators, characterization of 3D printed and cast chitosan as well as cast gelatin was conducted through mechanical tests and swelling ratio measurements. The bending measurements of actuators as an index of their performance were defined and experimental setup for conducting the experiments was developed. The actuation performances of all the actuators were measured and compared to reveal the actuation improvement achieved by 3D printing fabrication. Parametric modeling was used to estimate and simulate the dynamic behavior of actuator bending in response to electrical input.

Fabrication of the actuator

Using chitosan for printing purpose is preferable due, in part, to its rheological properties during printing and also its mechanical properties both at dry and hydrated states. In fact, the excessive number of charged groups in the backbone of polyelectrolytes (such as polyacrylic acid) results in straight chains of the polymer without significant entanglement even at high molecular weights. In other words, it can be said that the lack of sufficient entanglements among polymer chains severely limits their solution or melt processing for direct printing purposes. Such polyelectrolytes are highly hydrophilic, making their solution processing extremely difficult. They do not solidify fast enough or maintain integrity of the construct in extrusion-based technology like 3D printing that relies on rapid solidification of the extrudate. Therefore, it would be hard to achieve reproducible fabrication of uniform structures (similar to what is shown in our work) with a 3D-Bioplotter, while maintaining resolution among extruded filaments. Chitosan, in contrast, has limited number of charged groups. This limitation, although resulted in slower actuation, provided a viscous and extrudable solution that finally resulted in robust construction of filaments in direct ink printing.

Medium molecular weight chitosan (with 75–85% deacetylation degree) and acetic acid were purchased from Sigma Aldrich (Australia). A mixture of 1.6 g chitosan in 0.8 mL acetic acid (1 v/v%) was prepared under vigorous stirring at 50°C for 2h. This solution was poured into petri dishes and dried in an oven at 50 for 48 h to form the gel. The product then was rinsed in distilled water to remove any unreacted acetic acid for 2 days and dried again in an oven at 50°C for 48 h. The chitosan bar with size $24\times4\times1$ mm was cut precisely.

The flowchart of polyelectrolyte actuator printing is illustrated in Figure 2. Having prepared the ink, it was

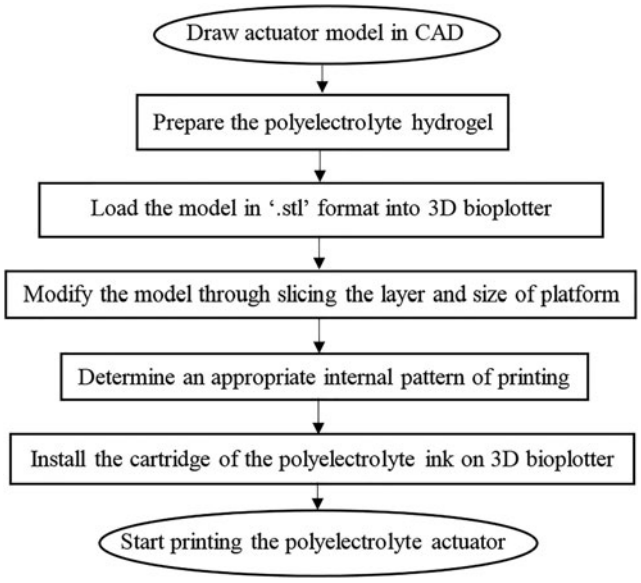

FIG. 2. Flowchart of printing the polyelectrolyte actuator using the 3D-Bioplotter. CAD, computer-aided design.

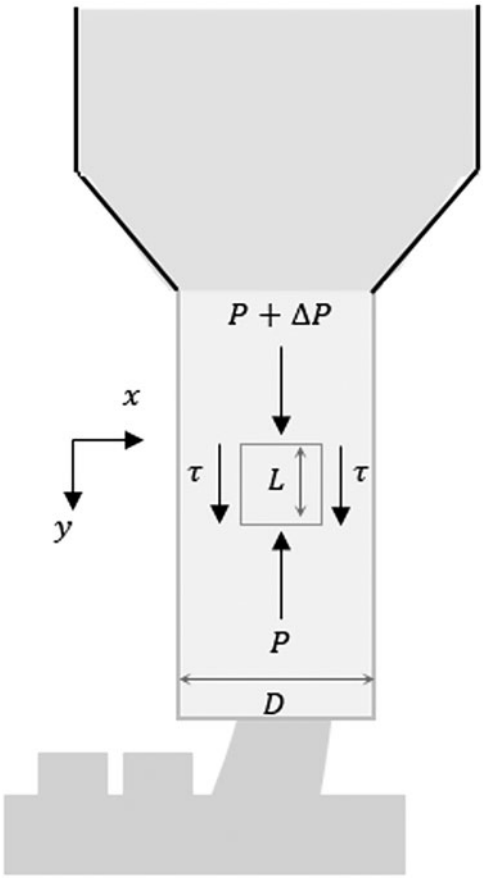

FIG. 3. Forces applied on an element in a nozzle.

sonicated to remove the bubbles to prevent them from deteriorating the quality of the print. Then, the solution was centrifuged and poured into low-temperature 3D-Bioplotter 30 cc syringe. A CAD model of the actuator was drawn in Solidworks (Dassault Systemes). Afterward, the generated file was imported to an EnvisionTEC GmbH 3D-Bioplotter (EnvisionTEC, Gladbeck, Germany). The CAD model was then printed without any support material. Ethanolic sodium hydroxide (EtOH–NaOH) with a recipe of 0.25 M NaOH (Sigma Aldrich), 70 v/v% EtOH ratio of 3:7, was used for postprinting solidification. During the printing process, the EtOH–NaOH is spinkled on the printed chitosan under room temperature to gelate it into a solid gel rapidly.

Gelatin can also be used as another polyelectrolyte polymer to be compared with chitosan in terms of soft polyelectrolyte actuators. Gelatin is a thermoresponsive polymer that becomes gel at $\sim$25°C, and its melting point is 37°C. It has been impractical to fabricate a 3D structure of gelatin utilizing our current 3D-Bioplotter, because a printed gelatin droplet on the printed stage would spread before solidification and the resulting material could not really be considered as 3D printed due to lack of distinctive structure and porosity. The printed gelatin did not remain intact but spread due to low viscosity before solidification. Indeed, a Peltier device that can control temperature of the impact point on the platform can be investigated as a future investigation on gelatin printing. Therefore, cast method for fabrication of gelatin actuator was used in this study. The gelatin actuator, made from gelatin from porcine skin, was purchased from Sigma Aldrich, Australia. Gel-forming solution was obtained by dissolving 4%w/w concentration of gelatin and deionized water and heated to 50°C, stirring continuously until homogenized. Gelatin solution was then poured into petridish and cooled at room temperature to form the gels. The gelatin bars were precisely cut to the size of $24\times4\times1$ mm.

Optimizing the printing parameters

To achieve best shape fidelity of printed polyelectrolyte actuator hydrogels, much effort is required to determine the optimum printing parameters. Optimizing the printing parameters requires an understanding of the relationships between the variables. Printing accuracy is defined by quality of printed strand that is consequential to shape fidelity and refers to strand width here.

The 3D-Bioplotter is a pneumatic extrusion dispenser system in which the shear stress of hydrogel in nozzle (τ) can be obtained by deriving equilibrium of forces on the fluid element along y axis shown in Figure 3 as

$$\tau(\pi DL) = (\mathrm{P} + \Delta P)\left(\pi D^2/4\right) - P\left(\pi D^2/4\right) \tag{5}$$

$$\tau = \frac{D\Delta P}{4L}, \tag{6}$$

where D, L, and ΔP are needle diameter, needle length, and extrusion pressure applied through nozzle. Knowing the viscosity of hydrogel (μ), shear stress can be found as a function of shear rate ($\dot{\gamma}$) as

$$\tau = \mu\dot{\gamma}. \tag{7}$$

Also, the relationship between volumetric flow rate ($\dot{q}$) and shear rate in a shear thinning fluid can be found from

$$\dot{q} = K\frac{\dot{\gamma}\,\pi D^3}{32}, \tag{8}$$

where K is the power law index coefficient that is assumed to be a constant value for a laminar flow.[31] The diameter of extruded hydrogel strand (d) can be assumed constant after printing to relate the shear rate to velocity of nozzle (V) in x direction as

$$\dot{q} = V\left(\frac{\pi d^2}{4}\right). \tag{9}$$

From Equations (8) and (9), shear rate can be written as

$$\dot{\gamma} = K\frac{8V\,d^2}{D^3}. \tag{10}$$

Finally, combination of Equations (6), (7), and (10) and rearranging it based on diameter of printed hydrogel strand yield

$$d = D^2\sqrt{\frac{K\Delta P}{32V\mu L}} \propto \sqrt{\Delta P} \propto \frac{1}{\sqrt{V}}. \tag{11}$$

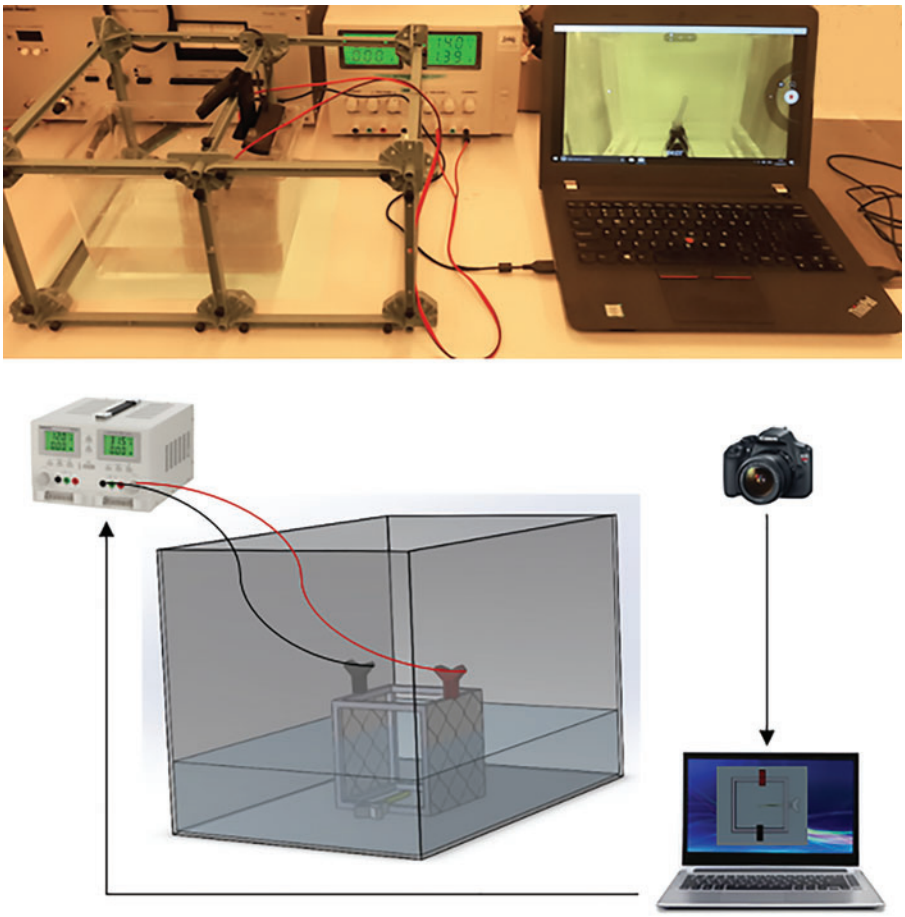

FIG. 4. Experimental setup. Color images available online at www.liebertpub.com/3dp

The optimization design is developed by understanding that the actuator would be printed in ambient laboratory temperature (20.°C) using a specified needle (constant needle diameter). Therefore, there would be two key factors: nozzle speed (V) and extrusion pressure (ΔP), to control printed strand width where per Equation (11) the extrusion pressure and speed of the nozzle are, respectively, proportional and inversely proportional to the width of the printed strand. Several experiments have been conducted to study the relation in Equation (11), where the objective was to achieve the optimum line width of hydrogel strand (closest to needle diameter) with the minimum extrusion pressure and nozzle velocity, which were studied in ranges 0.4–0.8 bar and 20–30 mm/s, respectively.

Mechanical tests

Determining true mechanical properties of polyelectrolyte hydrogels is not always straightforward because of their inherent complex mechanical behavior and low elastic modulus (of the order of 100 kPa). Polyelectrolyte hydrogels

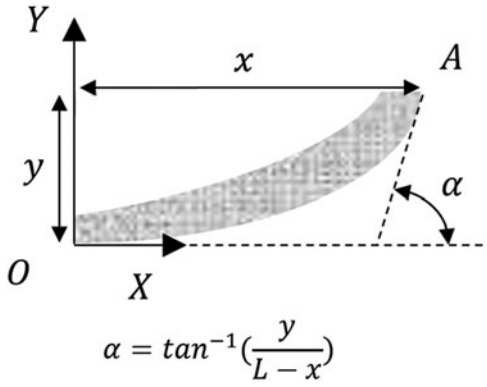

FIG. 5. Bending measurement of actuator.

TABLE 1. STRAND WIDTH RESULTS FROM 3D-BIOPLOTTER

Print sample No.	*Extrusion pressure/ΔP (bar)*	*Nozzle velocity/V (mm/s)*	*Strand width (mm)*
1	0.4	20	Discontinuous
2	0.4	25	Discontinuous
3	0.4	30	Unextruded
4	0.6	20	0.340
5	0.6	25	0.290
6	0.6	30	Irregular
7	0.8	20	0.450
8	0.8	25	0.400
9	0.8	30	0.320

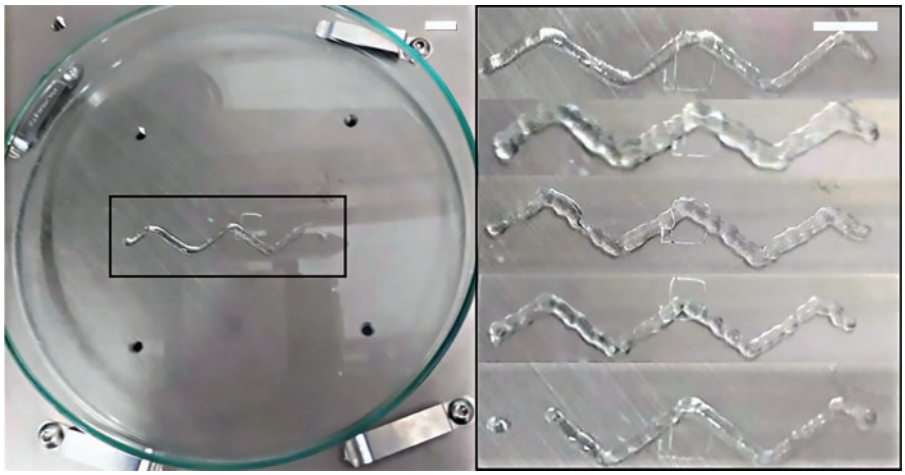

FIG. 6. Printed chitosan hydrogel strand. Sample Nos. 5, 7, 9, 4, and 6 are in order illustrated from *top*. The length of scale bars is 1 mm. Color images available online at www.liebertpub.com/3dp

are ductile materials that typically show large deformations. However, they can exhibit brittle fracture at high strain rates.[32] The basic mechanical properties of the dry hydrogels were analyzed by tensile testing. Young's modulus and yield strength of the cast film gelatin, cast film chitosan, and 3D printed chitosan hydrogel actuators were evaluated from the stress–strain graphs from the tensile test according to ASTM D638 (Type V) using a universal testing machine (Model: 5966; Instron). The tests were conducted with a load cell of 10 kN and crosshead speed of 2 mm/min, under the same conditions (ambient room temperature). Three dry replicates with dimensions of $22 \times 4 \times 1$ mm were tensile tested to obtain an average value of data. Owing to the wafer-like morphology of the 3D printed chitosan, the effective area of the cross section of the tensile specimen was evaluated and used in the calculations of the tensile stress.

Swelling measurements

Fluid uptake is an important factor in estimating the swelling behavior of hydrogel, which, in turn, can be a good indicator in assessing the movement performance of the 3D printed and cast film polyelectrolyte actuators in aqueous media. The swelling performance of the actuators was analyzed by measuring the liquid absorption as a function of time. Identical dehydrated samples for each type of actuator used for swelling studies were accurately weighed and immersed in 20 mL of 0.1 M NaOH at $20°C \pm 2°C$ until the swelling equilibrium was achieved.[32] At certain intervals of time, samples were taken out from the 0.1 M NaOH solution, blotted using absorbent paper, weighed, and immersed in the solution again. The water uptake was gravimetrically calculated by the following equation:

$$W_a\% = \frac{W_t - W_o}{W_o} \times 100, \tag{12}$$

where W_0 and W_t are the weights of dry and wet samples after time t, respectively. The measurements were conducted at five replicates.

Table 2. 3D-Bioplotter Settings for Printing Chitosan Actuator

Parameter	*Value*
Needle size (mm)	0.250
Layer thickness (mm)	0.2
Transfer height (mm)	5
Speed (mm/s)	25
Pressure (bar)	0.6
Temperature (°C)	20
Preflow delay (s)	0.05
Postflow delay (s)	0.05

Bending measurements

The electromechanical performance of the cast films of gelatin and chitosan, and 3D printed chitosan polyelectrolyte hydrogel actuators was assessed by immersing them in a 0.1 M NaOH solution with two contactless, parallel stainless steel electrodes situated 40 mm apart while the actuator is clamped in the center between electrodes. An electrical stimulus of 10 V was applied to the electrodes to generate the actuation motion on the actuator. A ''forward'' and ''reversed'' stimuli each lasting 180 s were applied to the electrodes. The extent of bending of the actuator tip was recorded by using a Logitech C920 webcam (Logitech International SA, Newark, CA) mounted on a retort stand. Recorded images were processed to produce a trajectory of the actuator tip (Fig. 4). In this study, a combination of tangent and curved components was used as the bending index α, where L is the length of the actuator (Fig. 5).

Parametric modeling

The 3D printed polyelectrolyte soft actuator generates highly nonlinear displacements when electrically stimulated due to its multidomain—electrical, chemical, and mechanical—properties. Thus, it is desired to incorporate these properties in a unified model describing their dynamic behavior under an electrical input. However, such a model to

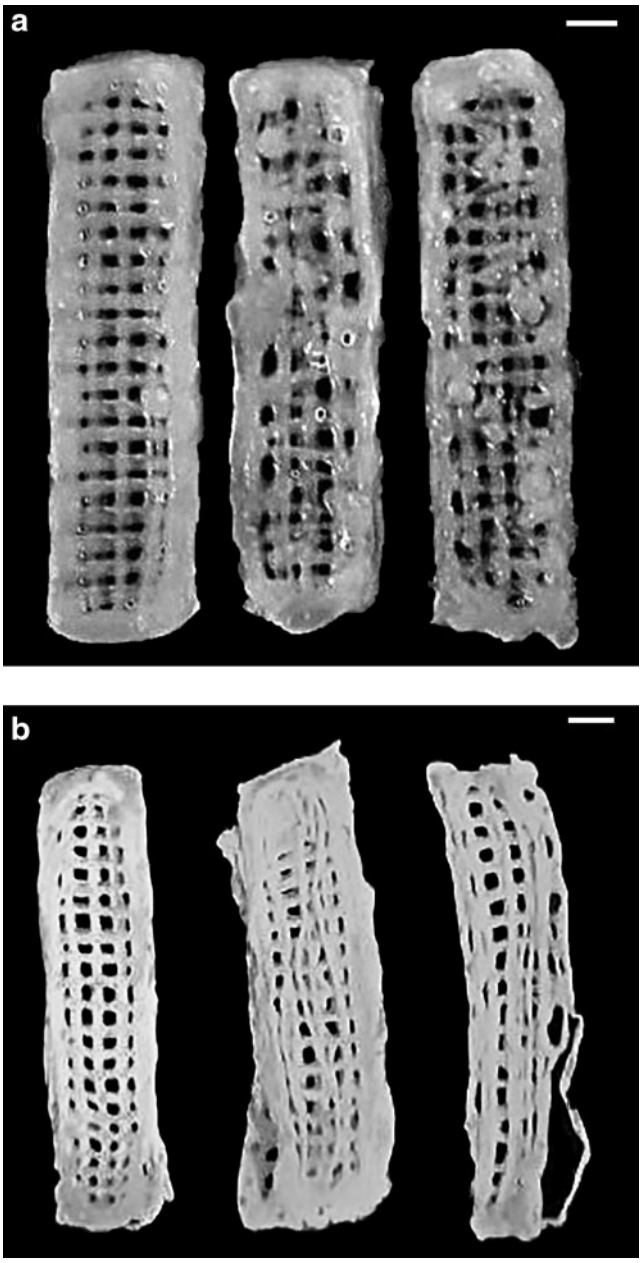

FIG. 7. Printed chitosan samples with different printer parameters (optimized parameters, high pressure, and high velocity from *left* to *right*, respectively); **(a)** just printed, **(b)** dried actuators. The length of scale bar is 3 mm.

understand the dynamic behavior of the actuator in the time domain will be quite complex to establish and computationally expensive. Despite some position control studies in the literature, those methods are not deemed appropriate since they merely focus on predesigned shapes that restrict the shape of a soft robotic manipulator, therefore, contradicting the wide-ranging design possibilities of soft actuators using 3D printing. Considering all these factors, a planar parametric model of soft actuator is utilized here.

A parametric kinematic model is presented only to determine the endpoint position of the actuator from its initially planar configuration as a function of time for a given input

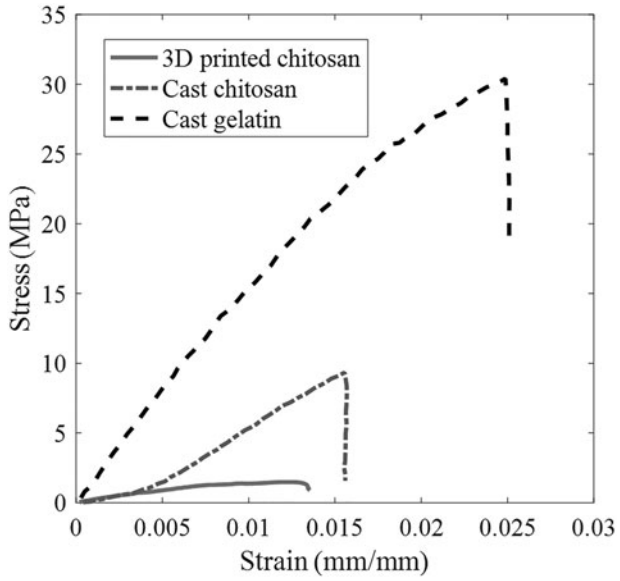

FIG. 8. Mechanical test results for the cast gelatin, cast chitosan, and 3D printed chitosan actuators.

voltage.[33] A polynomial function has been used for the parametric model, which is expressed as

$$\begin{bmatrix} X \\ Y \end{bmatrix} = \begin{bmatrix} A_n t^n + A_{n-1} t^{n-1} + \ldots + A_1 t + A_0 \\ B_{n-1} t^{n-1} + B_{n-1} t^{n-1} + \ldots + B_1 t + B_0 \end{bmatrix}, \quad (13)$$

where t is time, A_n and B_n are the input voltage-dependent coefficients for a specific electrical input.

Results and Discussions

Optimizing the printing parameter results

Table 1 gives various widths of the printed chitosan hydrogel strands with the same needle size (0.250 mm) at

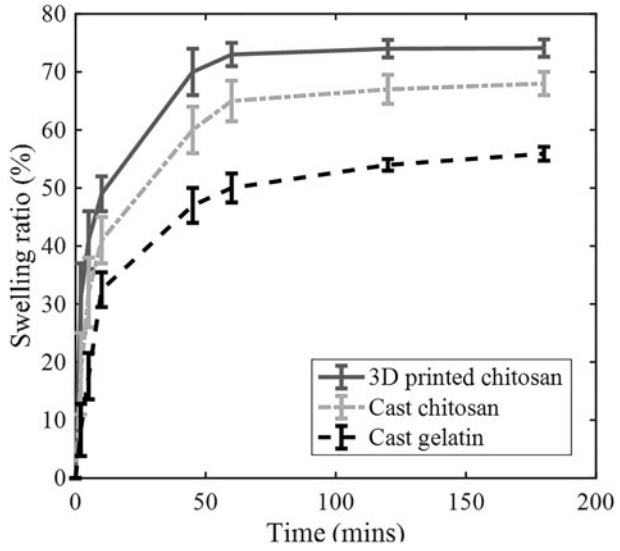

FIG. 9. Liquid uptake of the cast gelatin, cast chitosan, and 3D printed chitosan actuators. All bars indicate the standard deviation ($n=3$).

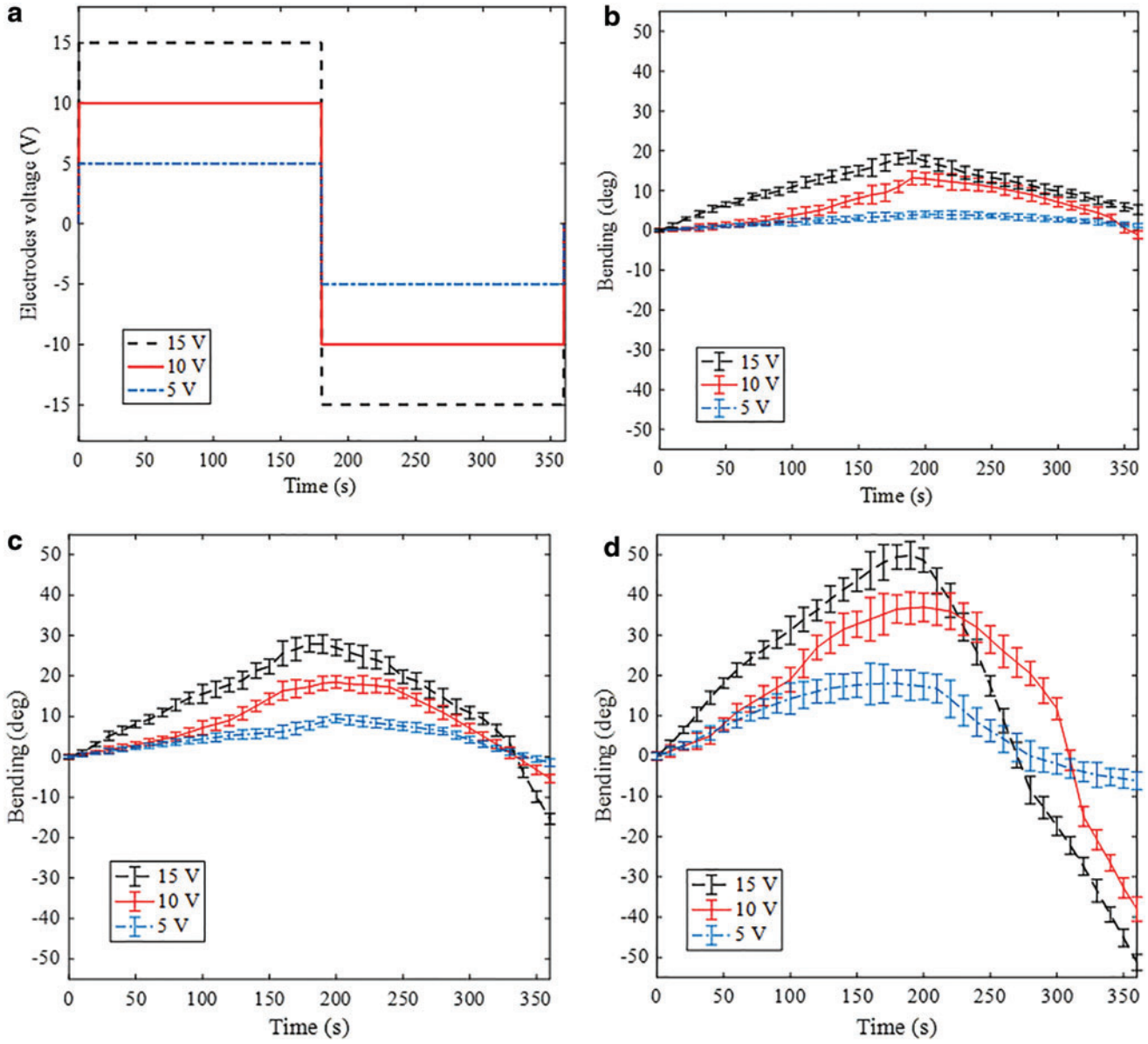

FIG. 10. Bending of hydrogels as a function of the electric field strength in 0.15 M NaOH solution, **(a)** electrodes input voltages, **(b)** cast gelatin actuator, **(c)** cast chitosan actuator, **(d)** 3D printed actuator. All bars indicate the standard deviation ($n=3$). Color images available online at www.liebertpub.com/3dp

different extrusion pressures and printing speeds. The width of the printed strand was found to be effectively controlled by varying the 3D printing setup, including the extrusion pressure and nozzle velocity. From the results shown in Figure 6 and Table 1, it can be deduced that, to get an optimum continuous line, the pressure must be sufficient to dispense a continuous strand at the given speed. However, when there is too much pressure, the width of hydrogel strand becomes much larger than the needle size. Another interesting observation is that, at a higher nozzle speed, the printed hydrogel had more defects than the hydrogel line that was printed at a lower speed. Ultimately, it was found that the optimum width of the printed strand is achieved as 0.290 mm at the extrusion pressure and nozzle speed of 0.6 bar and 25 mm/s, respectively.

Having established the optimum parameters of 3D-Bioplotter, the porous chitosan beam with the size of $40\times10\times5$ mm was printed. By keeping the chitosan ink at a constant temperature of 20°C and using a syringe as the extrusion system, the material deposited was consistent and predictable. Parallel strands were printed in one layer using the optimized parameter given in Table 2. For the next layer, the direction of the strands was turned 90° to the center of the object, creating a mesh with good mechanical properties, and mathematically defined porosity. The optimized values of 3D-Bioplotter print settings were determined through several printing tests (Table 2). Printed chitosan samples with different printer parameters can be seen in Figure 7.

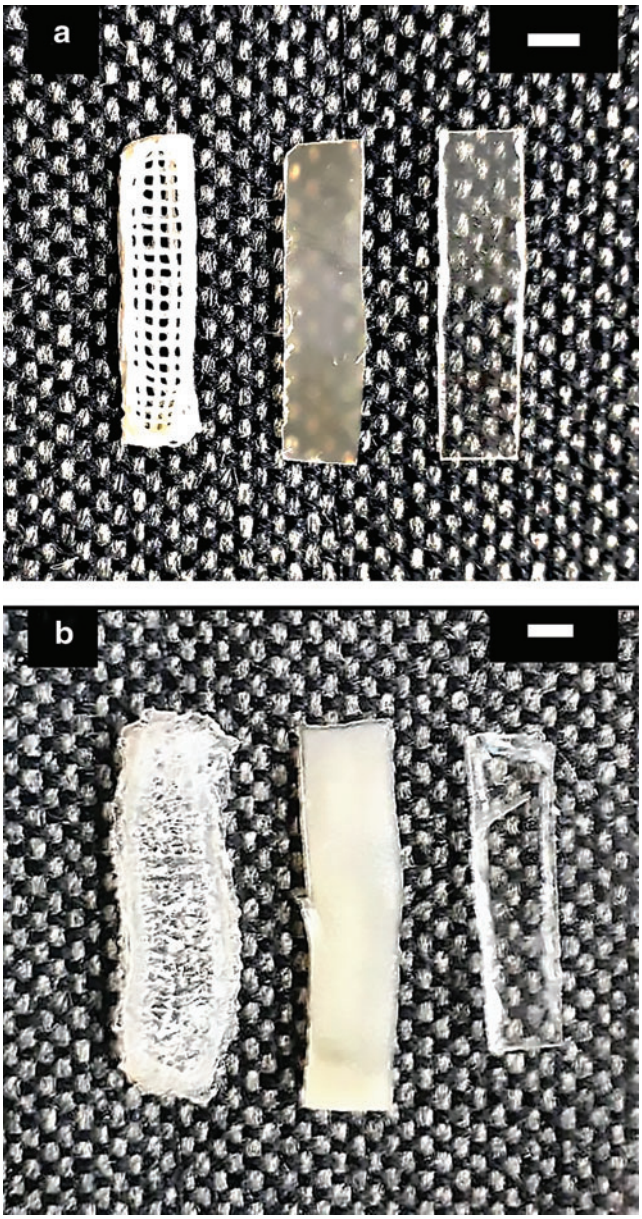

FIG. 11. 3D printed chitosan, cast chitosan, and cast gelatin from *left* to *right*; **(a)** before actuation **(b)** after actuation. Length of scale bars is 3 mm. Color images available online at www.liebertpub.com/3dp

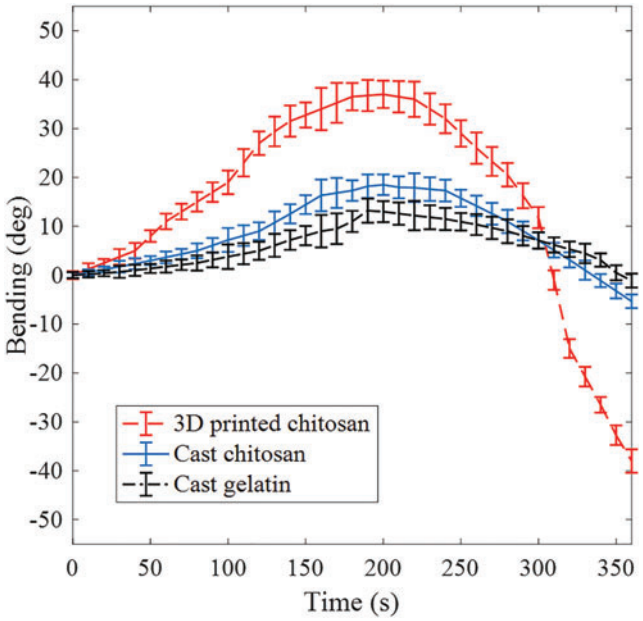

FIG. 12. 3D printed chitosan versus cast gelatin and chitosan actuators. All bars indicate the standard deviation ($n=3$). Color images available online at www.liebertpub.com/3dp

Mechanical tests results

Figure 8 shows the stress–strain plots of the hydrogels tested under same conditions. From these results, Young's moduli of the cast gelatin, cast chitosan, and 3D printed chitosan were found as 2.012 ± 0.006 GPa, 0.941 ± 0.004 GPa, and 71 ± 2 MPa, respectively. The tensile strength of the cast gelatin, cast chitosan, and 3D printed chitosan was also 30.2 ± 0.2, 9.2 ± 0.2, and 1.5 ± 0.1 MPa, respectively. The average standard deviation of the slope at modulus for the specimens was 0.0022, 0.0096, and 0.0708 MPa for the cast gelatin, cast chitosan, and 3D printed chitosan, respectively.

Compared with the 3D printed sample, the cast film polyelectrolyte hydrogels exhibited higher tensile strength and ductility. Cast gelatin was found to be strong whereas cast chitosan was stronger than 3D printed chitosan but not as strong as cast gelatin. Also the percentage elongation to break of printed chitosan sample was less than that of cast gelatin. The higher strength of the cast film polyelectrolyte samples can be attributed to more homogeneous structure of cast film than the 3D printed lattice film. In other words, unevenness in the 3D printing pattern can cause weakness due to uneven stress distributions and local stress concentrations, leading to early failure.

Swelling measurement results

The swelling performance of the cast gelatin films and chitosan and 3D printed chitosan was analyzed by measuring the swelling ratio results. Three identical dehydrated samples with dimensions of $22 \times 4 \times 1$ mm for each type of actuator used for swelling studies were accurately weighed and immersed in 20 mL of 0.1 M NaOH at $20°C \pm 2°C$ until the swelling equilibrium was achieved. The measurements were conducted at five replicates. All samples exhibited typical swelling behavior during early minutes of immersion. After a rapid rise, $W_a\%$ reached a plateau. The amount and trend of water absorption until equilibrium are shown in Figure 9. The hydrogel samples reached an equilibrium state after 120 min. Although the samples showed almost the same absorption trend before equilibrium, the 3D printed actuator exhibited significant enhancement of water absorption, particularly after 60 min, compared with the film cast actuators, indicating a higher mass transfer rate in the 3D printed hydrogels. For the same polymer and liquid conditions, this enhancement can be attributed to higher effective mass transfer area of the reticular 3D printed structure in comparison with the flat-structure cast specimen.

Actuation performance

The bending behavior of the polyelectrolyte hydrogel actuators is induced by the ionic gradient that is driven by an electric field. The motion of the counterions originated by the Donnan effect that can create an ionic concentration gradient within the hydrogel networks along the direction of the electric field. This results in an osmotic pressure difference within the hydrogel structure and consequently causes a deformation of the structure. Therefore, the effect of electrolyte concentration is a crucial factor on the bending behavior of the polyelectrolyte actuators. However, this factor has already been studied broadly in the literature and found that there is an optimum value of ionic concentration for each polyelectrolyte to reach its maximum bending. In this study, this was not our main concern but to study the effects of manufacturing on two different polyelectrolyte hydrogels with respect to their actuation performance. Another factor affecting the bending of actuator is the magnitude of electric voltage applied to the electrodes. It is expected that the degree of bending of the hydrogel is related to the counterion migration rate as well as to the increase of voltage. The increase in the counterion migration rate increases the hydrogel bending angle and rate of actuation.

The effect of the magnitude of the input voltage on the actuation behavior of cast gelatin and chitosan film and 3D printed chitosan hydrogel actuators was studied using $24 \times 4 \times 1$ mm samples with ionic strength of 0.15 M NaOH aqueous solution. The voltage between the electrodes was set to 5, 10, and 15 V, respectively, and the concentration of NaOH aqueous solution was kept constant at 0.15 M. It can be seen in Figure 10 that increasing the electrical voltage applied on the actuator increased the bending of the all actuators. Also, the bending gradient was quite high initially but decreased over time when the actuator reached its equilibrium state. This behavior could be observed more clearly at the reverse cycle. When the results of actuations are compared with the swelling rates, it is evident that with the increase of immersion time, a saturated state is approached, and is shown more clearly in reverse mode of applied voltage, where there is a decrease in the actuation response to the stimulus. This suggests that there is a decay in bending rate of actuators over time. The swelling and physical changes of the actuations before and after immersing in solution and actuation can also be seen in Figure 11.

To investigate the significance of 3D printing and its impact on the actuation performance of polyelectrolyte hydrogel actuators, a comparison was made between the actuation behavior of same-size actuators comprising two cast films of gelatin and chitosan and one 3D printed chitosan (Fig. 12). The bending angle of the actuators versus time over a full ''forward'' and ''reverse'' cycle of 360 s is acquired and shown in Figure 12. It can be deduced that the porosity imparted from the layer-by-layer 3D printing contributes to higher bending and actuation rate considerably. Also, closer examination of Figure 12 shows that despite existing discrepancy between the actuation rate of cast gelatin and chitosan, they follow quite similar trends compared with the 3D printed chitosan.

Furthermore, visual comparison of actuation between cast gelatin, cast chitosan, and 3D printed chitosan over time is shown in Figure 13. It is clearly shown that the 3D printed

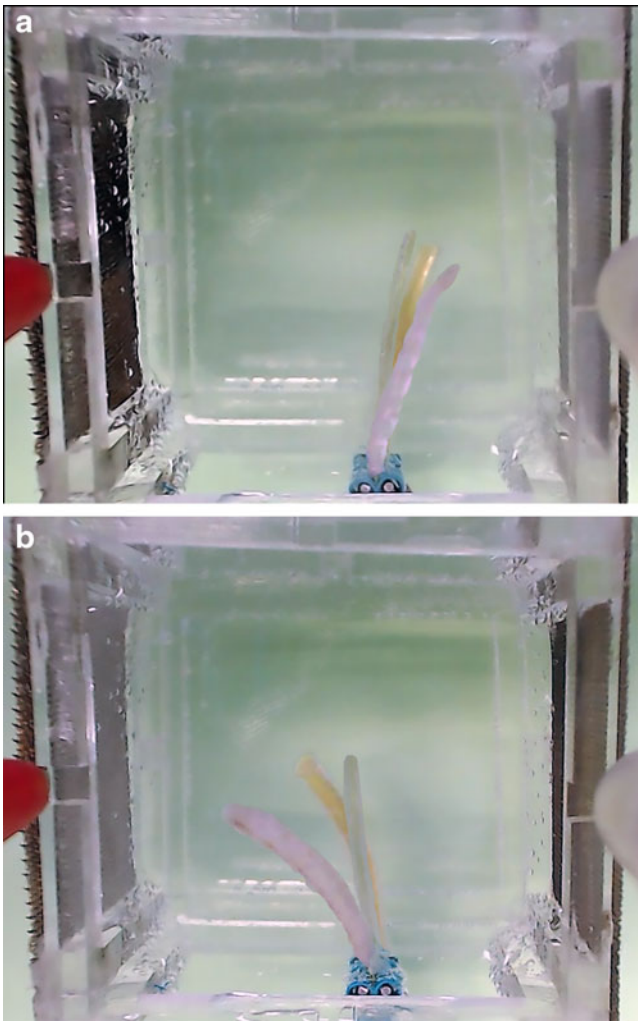

FIG. 13. Overlaid image sequences of the 3D printed chitosan, cast film chitosan, and cast film gelatin actuators in order of maximum bending; **(a)** after 120 s, **(b)** after 320 s. Color images available online at www.liebertpub.com/3dp

actuator showed a greater bending than both cast gelatin and chitosan when 10 V was applied first for 180 s and then for 180 s in a reverse polarity. It can be seen that in all states, the bending angle of 3D printed chitosan is higher than that of cast actuators.

The actuation performance of our 3D printed chitosan actuator was compared with that of the reported cast polyelectrolyte actuators.[2,4,29,34–36] Given that the printability of chitosan hydrogel is achieved under specific experimental parameters, it is not viable to draw exact comparisons with cast polyelectrolyte actuators that used different viscosity, electrolyte solution, and material concentration values. However, to provide an insight into the performance difference between the 3D printed chitosan actuator against the existing cast polyelectrolyte actuators, an evaluation of the maximum bending in response to different voltage increments is made. Table 3 presents the actuation performance of the 3D printed chitosan actuator against two existing cast polyelectrolyte actuators that reported maximum bending in response to different voltage increments and bending rates.[29,34] It was noted that the bending rate could be

Table 3. Actuation Performance of the 3D Printed Chitosan Actuator Against Two Existing Cast Polyelectrolyte Actuators

Type of actuators	Maximum bending angle increase (%) for input voltage increment (%)			Bending rate for 10 V (deg/s)
	100	150	200	
3D printed chitosan (this study)	135	60	265	0.19
Chitosan (this study)	80	55	250	0.09
Gelatin (this study)	100	60	235	0.06
Chitosan/poly(hydroxyethyl methacrylate)[34]	60	75	105	1.94
Synthesized acrylamide[29]	130	15	165	0.58

increased at specific voltage; however, the maximum bending angle with respect to voltage increment was limited in the existing works.[29,34] It can also be seen that higher values of maximum bending angle and bending rate for 10 V input could be achieved with the application of 3D printing in the fabrication of chitosan actuator, and this may also be applied to other polyelectrolyte actuators.

Overall, the results of experiments signify that the 3D printed hydrogel actuator was favorable for actuation because the lattice shape made in hydrogel cross-sectional area was such that a smaller electrical gradient was required across the hydrogel to provide the potential osmotic pressure required to initiate bending. Therefore, the performance of 3D printed actuators can be attributed to increased surface–to-volume ratio, flexibility, and increased Donnan effects across the hydrogel beam. However, as it was observed earlier in mechanical testing, these improvements were achieved at the expense of mechanical strength. This provides some flexibility at design level to emphasize the actuation and bending or mechanical strength, whichever is more critical.

Parametric model

A step voltage of 10 V was applied to stimulate the actuators for every test and their endpoint motion was captured with the camera. The tip positions of the actuator were extracted by analyzing the motion images. The parametric model was then obtained for the inverse kinematic calculation of all configurations of the actuator. The experimental and corresponding estimated endpoint positions of the 22-mm actuator under 10 V input, which were attained using the kinematic model, are shown in Figure 14. Two polynomials of fifth and seventh order were found to be best fitted for ''X'' and ''Y'' trajectories, respectively, when the actuator was stimulated by a full cycle comprising a 30 s forward and then immediate 30 s reverse input voltage of 10 V.

The parametric model given in Equation (14) estimates the actuator tip positions as a function of time for the given electrical input and describes the relationship between the electrical inputs and resulting output of the 3D printed actuator kinematics.

$$\begin{bmatrix} X \\ Y \end{bmatrix} = \begin{bmatrix} 1.22e-10t^5 - 9.94e-08t^4 + 2.50e \\ -05t^3 - 2.34e-03t^2 + 0.16t - 0.49 \\ -3.35e-11t^5 + 2.36e-08t^4 - 5.35e \\ -06t^3 + 4.69e-4t^2 - 0.02t + 24.03 \end{bmatrix} \quad (14)$$

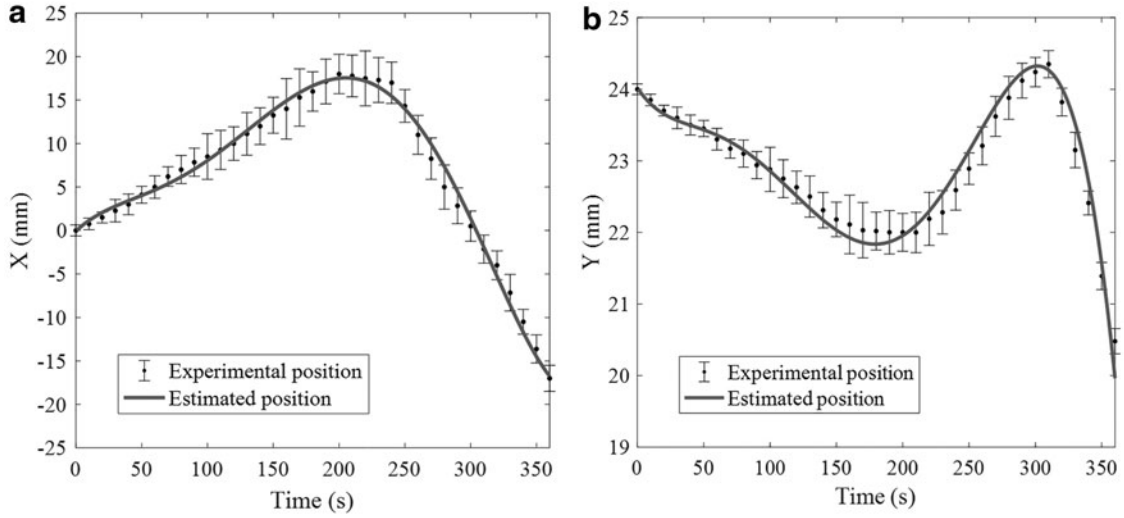

FIG. 14. Experimental and estimated tip positions of the 3D printed chitosan actuator; **(a)** x direction, **(b)** y direction. All bars indicate the standard deviation ($n=3$); goodness of fit for x, SSE: 25.4, R-square: 0.9914, RMSE: 0.9052; and for y: SSE: 0.6217, R-square: 0.9771, RMSE: 0.1416. SSE, sum squared error; RMSE, root mean squared error.

Conclusion

A novel application of 3D printing in polyelectrolyte soft actuators is presented in this study. It was observed that the contactless electroactive gelatin and chitosan demonstrated reversible bending with acceptable response time through polarity changes of electrodes over a 6 min cycle with one polarity change. Furthermore, chitosan was chosen to prove the concept of polyelectrolyte hydrogel actuator fabrication using 3D printing. The printing setup and parameters for layer-by-layer fabrication of the polyelectrolyte chitosan hydrogel actuator were optimized after rigorous testing considering 3D printing factors. It was shown that 3D printing improved the maximum deflection, and the deflection rate was compared with cast film gelatin as well as cast film chitosan. The rectilinear hollows made by 3D printing improved the deflection rate and ultimate deflection compared with the cast actuators with the same size. The multiphysics modeling and control of 3D printed polyelectrolyte actuator and 3D printing of off-the-shelf gelatin actuator could be interesting future research directions. Incorporating 3D printing and polyelectrolyte materials helps with custom-design flexibility and supports the renewable and sustainable robot concept.

Acknowledgments

The authors thank Jun Zhang (Institute of Frontier Materials, Deakin University) for assisting in 3D printing. This work was financially supported by the Deakin University Postgraduate Research Scholarship.

Author Disclosure Statement

No competing financial interests exist.

References

1. Winsberg J, Hagemann T, Janoschka T, *et al.* Redox-flow batteries: From metals to organic redox-active materials. Angew Chem Int Ed 2017;56:686–711.
2. Rossiter J, Winfield J, Ieropoulos I, *et al.* Here today, gone tomorrow: Biodegradable soft robots. SPIE Smart Structures and Materials+ Nondestructive Evaluation and Health Monitoring. Proc SPIE Int Soc Opt Eng Photonics 2016;9798:97981S.
3. Keller AG, Pham J, Warren H. Conducting hydrogels for edible electrodes. J Mater Chem B 2017;5:5318–5328.
4. Usta A, Asmatulu R. Synthesis and analysis of electrically sensitive hydrogels incorporated with cancer drugs. J Pharm Drug Deliv Res 2016;5:2.
5. Zhao G, Sun Z, Wang J, *et al.* Development of biocompatible polymer actuator consisting of biopolymer chitosan, carbon nanotubes, and an ionic liquid. Polym Compos 2017; 38:1609–1615.
6. Liu L, Jiang S, Sun Y, *et al.* Giving direction to motion and surface with ultra-fast speed using oriented hydrogel fibers. Adv Funct Mater 2016;26:1021–1027.
7. Shi X, Hu Y, Tu K, *et al.* Electromechanical polyaniline–cellulose hydrogels with high compressive strength. Soft Matter 2013;9:10129–10134.
8. Shang J, Shao Z, Chen X. Chitosan-based electroactive hydrogel. Polymer 2008;49:5520–5525.
9. Stoychev GV, Ionov L. Actuating fibers: Design and applications. ACS Appl Mater Interfaces 2016;8:24281–24294.
10. Altınkaya E, Seki Y, Yılmaz ÖC, *et al.* Electromechanical performance of chitosan-based composite electroactive actuators. Compos Sci Technol 2016;129:108–115.
11. O'Grady ML, Kuo P-L, Parker KK. Optimization of electroactive hydrogel actuators. ACS Appl Mater Interfaces 2009;2:343–346.
12. Migliorini L, Santaniello T, Yan Y, *et al.* Low-voltage electrically driven homeostatic hydrogel-based actuators for underwater soft robotics. Sens Actuators B 2016;228: 758–766.
13. Zhao Q, Dunlop JW, Qiu X, *et al.* An instant multi-responsive porous polymer actuator driven by solvent molecule sorption. Nat Commun 2014;5:4293.
14. Kim YS, Liu M, Ishida Y, *et al.* Thermoresponsive actuation enabled by permittivity switching in an electrostatically anisotropic hydrogel. Nat Mater 2015;14:1002–1007.
15. Tiyaboonchai W. Chitosan nanoparticles: A promising system for drug delivery. Naresuan Univ J 2013;11:51–66.
16. Jeon JH, Cheedarala RK, Kee CD, *et al.* Dry-type artificial muscles based on pendent sulfonated chitosan and functionalized graphene oxide for greatly enhanced ionic interactions and mechanical stiffness. Adv Funct Mater 2013; 23:6007–6018.
17. Zolfagharian A, Kouzani AZ, Khoo SY, *et al.* 3D printed hydrogel soft actuators. Region 10 Conference (TENCON). IEEE, Singapore, Singapore, 2016.
18. Campbell TA, Tibbits B, Garrett B. The Next Wave: 4D Printing Programming the Material World. Washington, DC: Atlantic Council, Technical Report. 2014.
19. Zolfagharian A, Kouzani AZ, Nasri-Nasrabadi B, *et al.* 3D printing of a photo-thermal self-folding actuator. KnE Eng 2017;2:15–22.
20. Zolfagharian A, Kouzani AZ, Khoo SY, *et al.* Evolution of 3D printed soft actuators. Sens Actuators A 2016;250:258–272.
21. Tibbits S, Cheung K. Programmable materials for architectural assembly and automation. Assembly Autom 2012; 32:216–225.
22. Gladman AS, Matsumoto EA, Nuzzo RG, *et al.* Biomimetic 4D printing. Nat Mater 2016;15:413–418.
23. Cvetkovic C, Raman R, Chan V, *et al.* Three-dimensionally printed biological machines powered by skeletal muscle. Proc Natl Acad Sci U S A 2014;111:10125–10130.
24. Mao Y, Ding Z, Yuan C, *et al.* 3D printed reversible shape changing components with stimuli responsive materials. Sci Rep 2016;6:24761.
25. Ozbolat IT, Hospodiuk M. Current advances and future perspectives in extrusion-based bioprinting. Biomaterials 2016;76:321–343.
26. Morales DH. Hydrogel Actuation by Electric Field Driven Effects. Dissertation. Raleigh, NC: North Carolina State University, 2015.
27. Shang J, Shao Z, Chen X. Electrical behavior of a natural polyelectrolyte hydrogel: Chitosan/carboxymethylcellulose hydrogel. Biomacromolecules 2008;9:1208–1213.
28. Flory PJ. Molecular configuration of polyelectrolytes. J Chem Phys 1953;21:162–163.
29. Li Y, Sun Y, Xiao Y, *et al.* Electric field actuation of tough electroactive hydrogels cross-linked by functional triblock copolymer micelles. ACS Appl Mater Interfaces 2016;8: 26326–26331.
30. Shiga T, Kurauchi T. Deformation of polyelectrolyte gels under the influence of electric field. J Appl Polym Sci 1990; 39:2305–2320.

31. Suntornnond R, Tan EYS, An J, *et al.* A mathematical model on the resolution of extrusion bioprinting for the development of new bioinks. Materials 2016;9:756.
32. Czerner M, Fasce LA, Martucci JF, *et al.* Deformation and fracture behavior of physical gelatin gel systems. Food Hydrocoll 2016;60:299–307.
33. Mutlu R, Alici G, Li W. Three-dimensional kinematic modeling of helix-forming lamina-emergent soft smart actuators based on electroactive polymers. IEEE Trans Syst Man Cybern Syst 2017;47:2562–2573.
34. Kim SJ, Shin SR, Lee SM, *et al.* Electromechanical properties of hydrogels based on chitosan and poly (hydroxyethyl methacrylate) in NaCl solution. Smart Mater Struct 2004;13:1036.
35. Yang S, Liu G, Wang X, *et al.* Electroresponsive behavior of a sulfonated poly (vinyl alcohol) hydrogel and its application to electrodriven artificial fish. J Appl Polym Sci 2010 15;117:2346–2353.
36. Arens L, Weißenfeld F, Klein CO, *et al.* Osmotic engine: Translating osmotic pressure into macroscopic mechanical force via poly (acrylic acid) based hydrogels. Adv Sci 2017;4:1700112.

Address correspondence to:
Abbas Z. Kouzani
School of Engineering
Deakin University
Geelong 3216
Victoria
Australia

E-mail: kouzani@deakin.edu.au